UC Irvine
UC Irvine Previously Published Works

Title

Development and evaluation of [125I]IPPI for Tau imaging in postmortem human Alzheimer's disease brain

Permalink

https://escholarship.org/uc/item/5pt2g2f5

Journal

Synapse, 75(1)

ISSN

0887-4476

Authors

Mukherjee, Jogeshwar
Liang, Christopher
Patel, Krystal K
et al.

Publication Date

2021

DOI

10.1002/syn.22183

Peer reviewed

Development and evaluation of [125I]IPPI for Tau imaging in postmortem human Alzheimer's disease brain

Jogeshwar Mukherjee, **Christopher Liang**, **Krystal K. Patel**, **Phuc Q. Lam**, **Rommani Mondal**

Preclinical Imaging, Department of Radiological Sciences, University of California, Irvine, CA, USA

Abstract

Objective: Alzheimer's disease (AD) is a neurodegenerative disease characterized by aggregation of Tau protein into paired helical filaments causing neurofibrillary tangles (NFT) in the brain. The aim of this study was to develop and evaluate the effectiveness of a novel radioiodinated tracer, 6-[125I]iodo-3-(1H-pyrrolo[2,3-c]pyridine-1-yl)isoquinoline ([125I]IPPI), for binding to Tau protein (Ki = 0.75 nM) in postmortem human brain (AD and cognitively normal (CN).

Methods: Radiosynthesis of [125I]IPPI was carried out by radioiododestannylation and purified chromatographically. Computational modeling studies of IPPI and MK-6240 binding on Tau fibril were evaluated. In vitro autoradiography studies were carried out with [3H]PIB for Aβ plaques and [125I]IPPI for Tau in AD and CN brains and evaluate drug effects.

Results: [125I]IPPI was produced in >95% purity. Molecular modeling of IPPI revealed binding energies of IPPI (−7.8, −8.1, −8.2, −7.5 Kcal/mol) at the four sites were comparable to MK-6240 (−8.7, −8.5, −8.3, −7.5 Kcal/mol). Ratio of average grey matter (GM) [125I]IPPI in AD versus CN was found to be 7.31 (p = .07) and AD GM/ white matter (WM) = 4.35 (p = .09). Ratio of average GM/WM [125I]IPPI in CN was 1.21. Binding of [125I]IPPI correlated with the presence of Tau, confirmed by anti-Tau Dako A0024. Specifically bound [125I]IPPI to Tau in AD brains was displaced by MK-6240 and IPPI (>90%). Monoamine oxidase inhibitors (MAO) inhibitors deprenyl and clorgyline effected [125I]IPPI binding at >1 μM concentrations.

Conclusion: [125I]IPPI exhibited high binding in human AD frontal cortex and anterior cingulate and is a suitable radioiodinated ligand for Tau imaging.

Keywords

[125I]IPPI; Alzheimer's disease; human Tau; neurofibrillary tangles

---

CONFLIC T OF INTEREST

The authors have no conflict of interest in the work reported here.

1 | INTRODUCTION

Alzheimer's disease (AD) is the most common type of dementia, accounting for 50 to 80 percent of dementia cases characterized by the accumulation of amyloid β (Aβ) plaques and neurofibrillary tangles (NFT) in the brain (Braak & Braak, 1991; Braak, Thal, Ghebremedhin, & Tredici, 2011). Several PET radiotracers have been developed for imaging of Aβ and some of them are currently in clinical use (Pan et al., 2016). Alongside progress in Aβ imaging, efforts have been underway on the development and use of NFT PET imaging agents (Lemoine et al., 2017). Current data suggests that in addition to Aβ imaging, NFT imaging can play an essential role in the clinical studies for evaluation of disease progression (Villemagne, Dore, Burnham, Masters, & Rowe, 2018). Selective diagnostic PET radiotracers can help in drug efficacy studies in relation to the development of the NFT (Leuzy et al., 2019). One of the earliest PET radiotracer was [^{18}F]FDDNP (Figure 1, **1**) which was less selective for NFT with higher levels of nonspecific binding (Chen et al., 2018). More selective PET radiotracers such as [^{18}F]THK5351 (Figure 1, **2**) provided useful information on AD patients, but have recently been reported to have significant off-target binding to monoamine oxidase (MAO B), reducing their potential use in AD diagnosis (Ng et al., 2017). Pyrrole derivatives such as [^{18}F]T807 (Figure 1, **3**) also appear to show some off-target MAO binding (e.g., Drake et al., 2019). Nevertheless, studies using [^{18}F]T807 and the related [^{18}F]RO6958948 (Figure 1, **4**) continue for NFT imaging in AD (Honer et al., 2018). Recently, a related radioiodinated derivative [^{125}I]pyridoimidazopyridine (Figure 1, **5**) has been developed for in vitro studies of NFT (Watanabe et al., 2020).

A second generation of NFT PET radiotracers based on azaindole structure, such as [^{18}F]MK-6240 (Figure 2, **6**), have been developed which bind to Tau protein more selectively and off-target binding to MAO using in vivo may not be a concern (Hostetler et al., 2016). These have high affinity and are capable of crossing the brain–blood barrier to be valuable for the application of in vivo NFT imaging in PET studies (Walji et al., 2016). As a NFT radiotracer, [^{18}F]MK-6240 shows characteristic changes in the brains of patients with AD (Betthauser et al., 2019). More recently, using autoradiographic studies, [^{18}F]MK-6240 has some propensity of being displaced by MAO inhibitors in vitro (Aguero et al., 2019).

Structure-activity studies of MK-6240 derivatives have been reported (Walji et al., 2015, 2016). Substituents at the six-position of the isoquinoline ring seem to have only a small effect on the binding affinity to Tau (Figure 2). Subnanomolar affinity was retained with no substituent (Figure 2, **8**, MK-H) while fluorine had a small increase in affinity (Figure 2, **7**, MK-10). Despite the better affinity of MK-10, fluorine-18 MK-F was found to be more lipophilic compared to [^{18}F]MK-6240 (Walji et al., 2016). The bulkier iodine showed a small decrease the binding affinity, but was still in the subnanomolar range (Figure 2, **9**, IPPI; Ki = 0.75 nM). Availability of an iodine-125 azaindole derivative for in vitro studies of NFT will be valuable to complement studies with [^{18}F]MK-6240. Therefore, our goal was to develop 6-iodo-3-(1H-pyrrolo[2,3-c] pyridine-1-yl)isoquinoline (IPPI) (Walji et al., 2015) as a suitable derivative for iodine-125 radiolabeling. In order to assess the value of 6-[^{125}I] iodo-3-(1H-pyrrolo[2,3-c]pyridine-1-yl)isoquinoline ([^{125}I]IPPI) in Tau imaging, we report here the following: (a) Synthesis of 6-iodo-3-(1H-pyrrolo[2,3-c]pyridine-1-yl)isoquinoline

(IPPI); (b) Radiosynthesis of 6-[^{125}I]iodo-3-(1H-pyrrolo[2,3-c]pyridine-1-yl)isoquinoline ([^{125}I]IPPI); (c) Molecular modeling of IPPI binding to Tau; (d) Comparison [^{3}H]PIB and [^{125}I]IPPI to postmortem AD human brain slices. (e) Evaluation of drug effects on the binding of [^{125}I]IPPI in postmortem AD human brain slices.

2 | MATERIALS AND METHODS

2.1 | General methods

All compressed gases were supplied by Airgas, Inc. Iodine-125 sodium iodide and [^{3}H]PIB were purchased from American Radiolabeled Chemicals, Inc., St. Louis, MO. Iodine-125 radioactivity was counted in a Capintec CRC-15R dose calibrator while low level counting was carried out in a Capintec Caprac-R well-counter. Specialty chemicals 2-chloro-6-iodoisoquinoline was obtained from 1Click Chemistry, New Jersey, MK-6240, 6-azaindole and 2-fluoro-6-bromoisoquinoline were purchased from AbaChemScene, New Jersey. Clorgyline and (R)-deprenyl were purchased from Research Biochemicals (Sigma Aldrich, St. Louis, MO). All other chemicals were obtained commercially from Sigma Aldrich, St. Louis, MO. All solvents used were provided by Fisher Scientific. For QC chemical purity, a Waters or Gilson HPLC system with UV detector set at 280 nm was used with 4.6×250 mm C18 Econosil reverse-phase analytical column was used. A semi-preparative HPLC column 100×250 mm 10 micron Econosil C18 reverse-phase was used.

Analytical thin-layer chromatography (TLC) was used to monitor reactions (Baker-flex, Phillipsburg, NJ, USA). Radio-TLC were scanned on an AR-2000 imaging scanner (Eckart & Ziegler, Berlin, Germany). Electrospray mass spectra were obtained from a Model 7250 mass spectrometer (Micromass LCT). Proton NMR spectra were recorded on a Bruker OM EGA 500-MHz spectrometer. Tritium was assayed by using a Packard Tri-Carb Liquid scintillation counter with 65% efficiency. Human postmortem brain tissue samples were obtained from Banner Sun Health Research Institute, Sun City, AZ brain tissue repository for in vitro experiments. Age and gender matched AD brain and cognitively normal (CN) brain tissue samples selected for end-stage pathology (Braak & Braak stage of VI; Braak & Braak, 1991). Human postmortem brain slices were obtained from chunks of frozen tissue on a Leica 1850 cryotome cooled to −20°C. Tritium and iodine-125 autoradiographic studies were carried out by exposing tissue samples on storage phosphor screens (Perkin Elmer MultiSensitive, Medium MS, and tritium sensitive phosphor screens). The apposed phosphor screens were read and analyzed by OptiQuant acquisition and analysis program of the Cyclone Storage Phosphor System (Packard Instruments Co., Boston, MA). All postmortem human brain studies were approved by the Institutional Biosafety Committee of University of California, Irvine.

2.2 | Synthesis

6-Iodo-3-(1H-pyrrolo[2,3-c]pyridine-1-yl)isoquinoline (IPPI), **9**:6-Azaindole, Figure 3, **10** (88 mg, 0.75 mmol) was treated with potassium *tert*-butoxide (115 mg, 1.03 mmol) in dimethylformamide (DMF, 3 ml) for 15 min at 120°C. Subsequently, 2-chloro-6-iodo-isoquinoline, Figure 3, **11** (289 mg, 1 mmol) was added to the reaction mixture and this mixture was then heated at 125°C for 24 hr. The mixture was then cooled, 10 ml of

water added and organics were extracted using dichloromethane (CH_2Cl_2). The CH_2Cl_2 layer was dried with anhydrous magnesium sulfate and purified using preparative TLC (CH_2Cl_2:CH_3OH 9:1) to provide IPPI, as an off-white solid **9** (61 mg, 0.18 mmol) in 24% yield. Spectral properties were similar to reported values (Walji et al., 2015). NMR (500 MHz, $CDCl_3$): δ 10.07 (s, 1H), 8.43 (d, $J = 5.3$ Hz, 1H), 8.22 (s, 1H), 8.19 (s, 1H), 8.01 (dd, $J = 4.5$, 0.86 Hz, 1H), 7.96 (d, $J = 3.45$ Hz, 1H), 7.86 (d, $J = 8.8$ Hz, 1H), 7.66 (s, $J = 8.8$ Hz, 1H), 7.61 (dd, $J = 4.5$, 0.86 Hz, 1H), 6.80 (d, $J = 3.4$ Hz, 1H). Mass Spectra (ESI): 372 ([M + H]$^+$, 100%), 743 ([2M + H]$^+$, 100%).

6-Bromo-3-(1H-pyrrolo[2,3-c]pyridine-1-yl)isoquinoline (BrPPI), **13**:6-Azaindole, Figure 3, **10** (100 mg, 0.85 mmol) was treated with potassium *tert*-butoxide (100 mg, 0.93 mmol) in dimethylformamide (DMF, 2 ml) for 15 min at 120°C. Subsequently, 2-fluoro-6-bromo-isoquinoline, Figure 3, **12** (100 mg, 0.44 mmol) was added to the reaction mixture and this mixture was then heated at 125°C for 24 hr. The mixture was then cooled, 10 ml of water added and organics were extracted using dichloromethane (CH_2Cl_2). The CH_2Cl_2 layer was dried with anhydrous magnesium sulfate and purified using preparative TLC (CH_2Cl_2:CH_3OH 9:1) to provide a light brown solid, BrPPI **13** (50 mg, 0.15 mmol) in 34% yield. NMR (500 MHz, $CDCl_3$): δ 9.62 (s, 1H), 9.27 (s, 1H), 8.39 (d, $J = 5.39$ Hz, 1H), 8.08 (s, 1H), 8.01 (dd, $J = 4.5$, 0.86 Hz, 1H), 7.91 (d, $J = 8.8$ Hz, 1H), 7.72 (d, $J = 8.8$ Hz, 1H), 7.69 (d, $J = 8.8$ Hz, 1H), 7.61 (d, $J = 5.37$ Hz, 1H), 6.78 (d, $J = 3.4$ Hz, 1H). Mass Spectra (ESI): 324 ([M + H]$^+$, 100%), 326 ([M + H]$^+$, 97%).

6-Tributyltin-3-(1H-pyrrolo[2,3-c]pyridine-1-yl)isoquinoline, **14**: To a solution of BrPPI, **13** (11 mg; 34 μmol) in anhydrous triethylamine (1 ml) under nitrogen, bistributyltin (60 mg; 103 μmol), and Tetrakis(triphenylphosphine)palladium(0) (5 mg; 4.3 μmol) were added. This reaction mixture was refluxed overnight at 88°C. Dark yellow crude reaction mixture was purified over prep silica gel TLC plate using hexane:ethyl acetate 1:1 as a solvent. Product with Rf = 0.5 was isolated (BrPPI Rf = 0.3) to yield pure tributyltin product **14** (4.5 mg; 8.4 μmol) as an oil (Figure 3, **14**) in 25% yield. NMR (500 MHz, $CDCl_3$): δ 9.65 (s, 1H), 9.25 (s, 1H), 8.38 (d, $J = 5.49$ Hz, 1H), 8.07 (s, 1H), 8.05 (s, 1H), 7.97 (d, $J = 8.0$ Hz, 1H), 7.80 (s, 1H), 7.72 (d, $J = 7.4$ Hz, 1H), 7.66 (d, $J = 5.4$ Hz, 1H), 6.81 (d, $J = 1.8$ Hz, 1H), 1.60 (m, 3H), 1.38 (m, 2H), 1.19 (t, $J = 8$ Hz, 2H), 0.92 (t, $J = 7.3$ Hz, 3H). Mass Spectra (ESI): 534 ([M + H]$^+$, 40%), 535 ([M + H]$^+$, 80%), 537 ([M + H]$^+$, 100%).

2.3 | Radiosynthesis

6-[^{125}I]iodo-3-(1H-pyrrolo[2,3-c]pyridine-1-yl)isoquinoline, 15 [^{125}I]IPPI: Radioiodination hood (CBS Scientific, Inc) placed inside a fume hood designated to handle radioactive materials was used to carry out all processes for radioiodination, separation, and purification. Iodine-125 radiolabeling was carried out by using modification of our previously reported radiolabeling procedures with iodine-123 and iodine-124 (Pandey et al., 2012; Pandey, Venugopal, Kant, Coleman, & Mukherjee, 2014). No-carrier-added Na^{125}I (18.5 MBq, approx 100 μl 0.01 N NaOH, 644 MBq/μg; American Radiolabeled Chemicals, St. Louis) was taken in a V-vial. To this vial 100 μl of 0.1 M sodium acetate/acetic acid buffer, pH 4 was added. This was mixed, and then, peracetic acid (50 μl, Sigma-Aldrich) was added and allowed to stand for 15 min at room temperature. Following this, tributyltin

precursor (Figure 4, **14**) 50 μg dissolved in 100 μl of ethanol was added and the reaction mixture was heated at 70°C for 0.5 hr. The vial was then cooled to room temperature and quenched by adding $NaHSO_3$ (100 μl of 1 mg/ml aq. stock) and saturated $NaHCO_3$ solution (200 μl) was added. The reaction mixture was then extracted with CH_2Cl_2 (2× 400 μl), dried ($MgSO_4$), evaporated (N_2 gas stream) to provide crude [^{125}I]IPPI, **15**. The crude mixture was purified on preparative TLC (CH_2Cl_2:CH_3OH 9:1) and separated from unreacted starting material. [^{125}I]IPPI, **15** was separated and extracted using ethanol. Radio-TLC of the ethanolic solution (Figure 4) showed purity >95% and Rf = 0.7 consistent with reference IPPI. This was ethanolic [^{125}I]IPPI, **15** at a concentration of 1 MBq/ml was used for in vitro experiments.

2.4 | Computational modeling IPPI binding to Tau

In order to assess binding of IPPI to Tau, we used the UCSF Chimera molecular modeling program (https://www.cgl.ucsf.edu/chimera). The reported cryo-EM three-dimensional (3D) structure of Tau fibril was used to perform molecular prediction on the Tau fibril (Fitzpatrick et al., 2017). The 3D model of Tau fibril consists of the paired helical filament (PHF) which is the principal component of neurofibrillary tangles in AD with the characteristic appearance is generated by a "double-helical stack of morphological units, each with a C-shaped cross-section displaying three domains" (Crowther, 1991).

The UCSF Chimera software is developed by the RBVI (Resource for Biocomputing, Visualization, and Informatics at the University of California San Francisco, USA) for interactive visualization and analysis of molecular structures. Along with AutoDock Vina it allows to perform molecular docking to predict the optimal molecular geometry of the tracers on the Tau fibril. AutoDock Vina offers three components to molecular docking: binding site identification, conducting a search procedure (a blind docking) to find the optimal binding sites and provide docking score that compare between the different binding conformation free energies in ligand-protein integration.

We performed blind docking of Tau tracers T807 and MK6240. The molecular structures for these tracers were built using the ChemDraw software (Ithacus software, Inc) and saved in. mol2 file format. They were optimized using the quantitative structure-activity relationships (QSAR) as implemented in AutoDock Vina software. After optimization, the tracer's molecular geometry was used for docking with Tau fibrils. The structures for the paired helical filament (protein database reference id is 5O3L) were used based on the recently reported cryo-EM technique (Fitzpatrick et al., 2017).

A blind docking with chosen grid box was selected to perform molecular docking. The grid box dimensions were chosen so that the surface sites in Tau fibrils were captured. The clusters corresponding to binding energies (represented by Kcal/mol) with the less negative scores were considered for analysis for the different binding sites (Murugan, Nordberg, & Agren, 2018). Binding of the Tau fibril by using Monte Carlo simulated annealing logarithm techniques were used for predicting minimal free energy binding to find optimal binding locations and to calculate docking score. These procedures were then used to evaluate the binding of IPPI to Tau.

2.5 | Postmortem human brain frontal cortex autoradiography

2.5.1 | [³H]PIB for Aβ—Human brain frontal cortex tissue from 6 AD and 6 cognitively normal (CN) subjects (Table 1, Banner Health Research Institute, Sun City, Arizona) were sectioned (10 μm thickness) on a Leica 1850 Cryostat and collected on Fisher slides. The slides contained three to four brain sections each were placed in separate glass chambers (six slides per chamber) were preincubated in PBS buffer for 15 min. The preincubation buffer was discarded, and then, to the chambers, [³H]PIB in 10% of ethanol PBS buffer pH 7.4 (60 ml; 74 kBq/ml), was added and the chambers were incubated at 25°C for 1 hr (Baranwal, Patel, & Mukherjee, 2014). Nonspecific binding was measured in separate chambers in the presence of 10 μM PIB. The slices were then washed with cold 10% of alcohol PBS buffer (2 × 3 min), cold deionized water 1 min, respectively. The brain sections were air dried, exposed overnight on a phosphor film, and then, placed on the Phosphor Autoradiographic Imaging System/Cyclone Storage Phosphor System (Packard Instruments Co). Regions of interest (ROIs) were drawn on the slices and the extent of binding of [³H]PIB was measured in digital light units, DLU/mm^2 using the OptiQuant acquisition and analysis program (Packard Instruments Co).

2.5.2 | [¹²⁵I]IPPI for Tau—Human brain frontal cortex tissue from the 6 AD and 6 cognitively normal (CN) subjects (Table 1) were preincubated in PBS buffer for 15 min. The slides contained three to four brain sections each were placed in separate glass chambers (six slides per chamber) were preincubated in PBS buffer for 15 min. The preincubation buffer was discarded, and then, to the chambers, [¹²⁵I]IPPI in 10% of ethanol PBS buffer pH 7.4 (60 ml; 3.7 kBq/ml), was added and the chambers were incubated at 25°C for 1.25 hr. Nonspecific binding was measured in separate chambers in the presence of 10 μM MK-6240. The slices were then washed with cold PBS buffer, 50% of ethanolic PBS buffer twice, PBS buffer, and cold water for 2,1,1,2,1 min, respectively. The brain sections were air dried, exposed overnight on a phosphor film, and then, placed on the Phosphor Autoradiographic Imaging System/Cyclone Storage Phosphor System (Packard Instruments Co). Regions of interest (ROIs) were drawn on the slices and the extent of binding of [¹²⁵I]IPPI was measured in DLU/mm^2 using the OptiQuant acquisition and analysis program (Packard Instruments Co).

2.6 | Drug effects on [¹²⁵I]IPPI postmortem human AD brain

Human anterior cingulate sections containing corpus callosum were sectioned from two AD subjects (Table 1). These sections were used to evaluate the effect of drugs on the binding of [¹²⁵I]IPPI to Tau. MK-6240 (10 μM) was used since it is known to bind to Tau and is an analog of [¹²⁵I]IPPI. Unlabeled IPPI (10 μM) was used to displace by using a saturating dose of 10 μM. BrPPI (10 μM), as a bromo analog of IPPI was used to ascertain binding to Tau. Monoamine oxidase (MAO) B inhibitor, (R)-deprenyl was used at two different concentrations (1 and 10 μM) and MAO A inhibitor, clorgyline was also used at two different concentrations (1 and 10 μM). The slides containing the sections (10 μm thick) were preincubated in PBS buffer for 15 min in eight different slide chambers (one total binding and seven with the different drugs). The preincubation PBS buffer was discarded and appropriate amount of each drug (dissolved in ethanol) was added to the chambers with the slides. To each chamber was then added [¹²⁵I]IPPI and 60 ml of 10% ethanolic PBS

buffer for a final concentration of 3.7 kBq/ml of [^{125}I]IPPI. The chambers were incubated at 25°C for 1.25 hr. The slides were then washed with cold PBS buffer, 50% of ethanolic PBS buffer twice, PBS buffer, and cold water for 2,1,1,2,1 min, respectively. The slides with the brain sections were air dried, exposed overnight on a phosphor film, and then, placed on the Phosphor Autoradiographic Imaging System/ Cyclone Storage Phosphor System (Packard Instruments Co). Regions of interest (ROIs) were drawn on the slices and the extent of binding of [^{125}I]IPPI was measured in DLU/mm^2 using the OptiQuant acquisition and analysis program (Packard Instruments Co).

Neighboring slices were immunostained with DAKO polyclonal antibody to total Tau which detects all six isoforms of Tau, dilution 1:3000, A0024 (Agilent, CA, USA) using reported protocols (Julien et al., 2012). For Aβ plaques, slices from all subjects were immunostained with anti-Aβ Biolegend 803015 (Biolegend, CA, USA) which is reactive to amino acid residue 1–16 of β-amyloid. Pictures were taken on a Trinocular microscope from AmScope, Inc.

3 | RESULTS

3.1 | Synthesis and radiolabeling

One step synthesis using 6-azaindole and 2-chloro-6-iodoisoquinoline provided moderate yields of IPPI. This is simpler than the two-step process involving diazotization of the nitro derivative previously reported (Walji et al., 2015), but simplifies the synthesis to a single step from commercially available starting materials. The synthesis of the bromo analog, BrPPI was carried out under similar one-step conditions as the synthesis of IPPI, but used 2-fluoro-6-isoquinoline. The yield was higher for BrPPI (34%) compared to IPPI (24%). For purposes of preparing the tributyltin precursor for radioiodinations, BrPPI was used. Using our previously published methods, the bromine was successfully substituted with tributyltin substituent in 25% yield, sufficient for use in radiolabeling procedures (Pandey et al., 2012, 2014).

Radiolabeling with sodium iodide-125 was carried out by using peracetic acid (PAA) as the oxidant. At room temperature, the reaction mixture was turbid, perhaps due to the low solubility of the tributyltin precursor. Radio-TLC monitoring showed little product. Upon heating the mixture at 70°C, the reaction mixture cleared up and Radio-TLC indicated formation of product, [^{125}I]IPPI. No other major radiolabeled organic side products were observed. Purification and isolation of [^{125}I]IPPI on preparative TLC worked efficiently, with little loss on the silica. Purity of the final isolated product was >95% as seen in the TLC autoradiograph as a single spot and the TLC chromatogram. The radiochemical yield of [^{125}I]IPPI was, however, low (<10%). Methods to improve radiochemical yield will be explored in order to produce [^{125}I]IPPI and its iodine-123 and iodine-124 analogs in high radiochemical yield and high-specific activity for in vivo studies. This may involve the use of alternate oxidants such as chloramine-T as well as adding some carrier iodide as was previously observed with our work on [^{123}I]Niodene (Pandey et al., 2012) and [^{124}I]epidepride (Pandey et al., 2014).

3.2 | IPPI-Tau molecular model

The reported cryo-EM three-dimensional (3D) structure of Tau fibril was used to carry out molecular interaction of IPPI on the Tau fibril (Fitzpatrick et al., 2017). The 3D model of Tau fibril consists of the paired helical filament (PHF) which is the principal component of NFT in AD with the characteristic appearance generated by a double-helical stack of morphological units, each with a C-shaped cross-section displaying three domains. Binding location and energy of binding (Kcal/mol) of various PET tracers for Tau fibrils are based on four main sites on the Tau fibril as reported by Murugan et al. (2018). Knowing the location of the binding site prior to docking can significantly increase the docking efficiency (Meng, Zhang, Mezei, & Cui, 2011).

Four binding sites were identified for the PET radiotracers MK-6240 and T807 (Murugan et al., 2018). We used the Chimera software to evaluate the binding energies of MK-6240 and T807 at these four binding sites and compared them with reported findings (Murugan et al., 2018). Figure 5a shows a good correlation of binding energy values (Kcal/mol) for the two compounds at the four sites using the Murugan method and our application of the Chimera method. The binding energies with the Chimera method were lower than the Murugan method, but they followed approximately the same profile for the four different sites. For MK-6240, the lowest energies were found for Site 1 in both methods, while for T807 the Chimera method was less discriminatory compared to the Murugan method for the Sites 1, 2, and 3 (Table 2). Binding of IPPI at the four sites is shown in Figure 5b. Binding energies at Sites 3 and 4 were similar to those of MK-6240, while Sites 1 and 2 were lower than MK-6240 (Table 2).

3.3 | Postmortem human AD brain autoradiography

Frontal cortex of 6 AD subjects and 6 CN subjects (Table 1) were used to evaluate the binding of [^{3}H]PIB for the presence of Aβ plaques and binding of [^{125}I]IPPI for the presence of Tau pathology. All brain sections contained grey matter (GM) and white matter (WM) regions (Figure 6a,f,k,p). Two AD subjects brain slices are shown in Figure 6b (female) and Figure 6g (male) with preferential binding of [^{3}H]PIB in the GM compared to the WM. Presence of Aβ plaques was confirmed with anti-Aβ IHC as shown in in Figure 6c,h. Shown in the plot in Figure 7a, all AD subjects exhibited higher GM binding of [^{3}H]PIB compared to WM, consistent with the presence of Aβ plaques. Brain slices from CN subjects are shown in Figure 6l (female) and Figure 6q (male) with little binding of [^{3}H]PIB in the GM and WM. This was confirmed with the absence of any significant anti-Aβ IHC as shown in Figure 6m,r. Shown in the plot in Figure 7a, all CN subjects exhibited lower GM binding of [^{3}H]PIB compared to that in AD, consistent with the absence of Aβ plaques. Inset in Figure 7a shows averages of all AD and CN subjects GM and WM. Ratio of average GM [^{3}H]PIB in AD versus CN was found to be 5.28 ($p < .001$) and AD GM/WM = 3.86 ($p < .001$). Ratio of average GM/WM [^{3}H]PIB in CN was 2.64 ($p < .05$). It should be noted that the AD WM exhibited higher levels of [^{3}H]PIB binding compared to CN subjects in Figure 7a.

Two AD subjects brain slices are shown in Figure 6d (female) and Figure 6i (male) with preferential binding of [^{125}I]IPPI to Tau in the GM compared to the WM. Presence of Tau

was confirmed with anti-Tau IHC as shown in Figure 6e,j. Shown in the plot in Figure 7b, all AD subjects exhibited higher GM binding of [^{125}I]IPPI compared to WM, consistent with the presence of Tau. However, there was greater variability of GM [^{125}I]IPPI binding in AD subjects compared to [^{3}H]PIB binding in the same subjects. Brain slices from CN subjects are shown in Figure 6n (female) and Figure 6s (male) with little binding of [^{125}I]IPPI in the GM and WM. Presence of Tau was confirmed with anti-Tau IHC as shown in Figure 6e,j. Shown in the plot in Figure 7b, all CN subjects exhibited lower GM binding of [^{125}I]IPPI compared to that in AD which was consistent with the absence of Tau shown in Figure 6o and T. Inset in Figure 7b shows averages of all AD and CN subjects GM and WM. Ratio of average GM [^{125}I]IPPI in AD versus CN was found to be 7.31 (p = .07) and AD GM/WM = 4.35 (p = .09). Ratio of average GM/WM [^{125}I]IPPI in CN was 1.21. It should be noted that the AD WM exhibited higher levels of [^{125}I]IPPI binding compared to CN subjects Figure 7b.

3.4 | Drug Effects postmortem human AD brain

Postmortem brain sections of two AD subjects (11–107 and 11–38, Table 1) were used to evaluate the effect of different drugs on Tau binding of [^{125}I]IPPI. All brain sections contained grey matter (anterior cingulate, AC) and white matter (corpus callosum, CC) regions (Figure 8a). The brain sections were characterized to have significant amounts of NFT by Banner Health with a total tangle score of 15. In the absence of any other drugs, significant [^{125}I]IPPI binding was observed in the GM comprising of AC, while the WM consisting of CC has little binding (Figure 8b). The ratio of AC to CC was >9. Upon addition of unlabeled IPPI (10 μM), most of the binding of [^{125}I]IPPI (>94%) to AC was abolished, as expected. In order to assess any off-target binding of [^{125}I]IPPI to MAO B, we used two concentrations, 1 and 10 μM of the competing drug, (R)-deprenyl (Mukherjee & Yang, 1997). The lower 1 μM of (R)-deprenyl had little effect on the binding of [^{125}I]IPPI (Figure 8c), but the higher 10 μM of (R)-deprenyl displaced approximately 13% of [^{125}I]IPPI binding. Similarly, to assess off-target binding of [^{125}I]IPPI to the other isozyme, MAO A, we used two concentrations, 1 and 10 μM of the competing drug, clorgyline (Mukherjee & Yang, 1999). The lower 1 μM of clorgyline had some displacing effect on the binding of [^{125}I]IPPI, while 10 μM of clorgyline displaced approximately 20% of [^{125}I]IPPI (Figure 8d). The bromo analog of IPPI, BrPPI (10 μM) displaced >96% of [^{125}I]IPPI binding from the AC suggesting high affinity for the Tau binding sites (Figure 8e). The high affinity PET radiotracer MK-6240 (10 μM) also displaced >95% of [^{125}I]IPPI binding in the AC suggesting similar binding sites of IPPI and MK-6240 (Figure 8f). Binding of [^{125}I]IPPI correlated very well with immunohistochemical findings of total Tau as seen in Figure 8h, thus, confirming binding of [^{125}I]IPPI to regions with Tau in the brain slice. The subjects also showed significant amounts of Aβ plaques, confirmed by anti-Aβ IHC (Figure 8g). Both subjects, 11–107 and 11–38, behaved similarly to the effects of the various drugs, summarized in (Figure 8i).

4 | DISCUSSION

There have been many recent advances in Tau imaging using PET in AD and other tauopathies. Several PET imaging agents have provided an extensive amount of information

on the gradual built up of NFT in disease progression of the AD brain. Some of the initial agents have now been shown to be less selective for Tau binding (Betthauser, 2019). The use of [18F]MK-6240, a second generation PET radiotracer, appears to be gaining more attention, since perhaps it may be more selective than previous agents. In pursuit of a radioiodinated analog of [18F]MK-6240, we evaluated [125I]IPPI as a potential candidate for Tau imaging. The major difference between the two is the lack of an amino group at the five-position and replacement of the fluorine by iodine. Interestingly, the amino group in [18F]MK-6240 was incorporated to decrease in vivo nonspecific binding by lowering lipophilicity of [18F]MK-10 (Walji et al., 2016). IPPI retains a high affinity for Tau (K_i = 0.75 nM), which is comparable to [18F]MK-6240 (K_i = 0.43 nM). Thus, it appears that the six-position of the isoquinoline ring is somewhat insensitive to halogen substituents.

Although the binding affinities of the four azaindole derivatives were close together in the subnanomolar range (Figure 2), it remained unclear if the large substituents (fluorine vs. iodine) might have an altering effect on the binding site. The recent elucidation of the three-dimensional structure of Tau from the AD brain using cryo-EM has provided valuable insights on molecular interactions (Fitzpatrick et al., 2017). Studies of molecular interactions of PET radioligands with this 3D Tau structure have now been reported (Goedert, Yamaguchi, Mishra, Higuchi, & Sahara, 2018; Murugan et al., 2018). For MK-6240 and T807, two commonly used PET radioligands, four binding sites have been reported (Murugan et al., 2018). We used the UCSF Chimera software for interactive visualization and analysis of molecular structures along with AutoDock Vina to perform molecular docking. Initially both MK-6240 and T807 were evaluated and compared to the findings of Murugan et al., 2018. Figure 5a shows a good correlation between our model parameters compared to the Murugan model for the four sites for both MK-6240 and T807. IPPI binding was then evaluated at the four sites (Figure 5b) and lowest binding energies were found in the order of Site 3 < Site 2 < Site 1 < Site 4 compared to MK-6240 which was found to be Site 1 < Site 2 < Site 3 < Site 4. In order to understand similarities/differences between MK-6240 and IPPI at the four binding sites, we compared their interactions by modeling both at the four sites (Figure 9). At Site 3, there appears to be complete overlap of MK-6240 and IPPI (Figure 9c) and at Site 1 interactions are similar and there does not appear to be any steric hindrance for the iodine atom (Figure 9a). At Site 4, the fluorine in MK-6240 and iodine in IPPI are interacting on opposite sides (Figure 9d) while in Site 2 the azaindole rings are on opposite sides (Figure 9b). Thus, it appears that there may be high degree of similarity of MK-6240 and IPPI at Site 3 followed by Site 1. There seem be more differences in interaction between MK-6240 and IPPI at Site 2 and Site 4. It should be noted that in our in vitro binding studies using AD brain slices, MK-6240 displaced >95% [125I]IPPI from the AC, suggesting good correspondence in the binding sites of the two radioligands.

For radiolabeling with iodine-123, we had previously evaluated two different oxidants, chloramine-T and peracetic acid and under conditions with added iodide (Pandey et al., 2012). Both oxidants provided low radiolabeling yields and the yields improved only when sodium iodide was added. In the present case of [125I]IPPI, we decided not to add any sodium iodide and carry out the radiolabeling under "no-carrier" conditions using peracetic

acid. Although the radiochemical yield of $[^{125}I]$IPPI was low, the radiochemical purity was very high (>95%, Figure 4).

In vitro binding of $[^{125}I]$IPPI was evaluated in 6 AD and 6 CN subjects. Frontal cortex of the subjects were first evaluated for the presence of Aβ plaques using $[^{3}H]$PIB and as expected all AD subjects showed the presence of Aβ plaques, whereas all the CN subjects had significantly lower $[^{3}H]$PIB binding. The AD subjects exhibited more than five times the amount of binding in the GM compared to CN subjects. The same subjects frontal cortex were then evaluated for the presence of Tau pathology using $[^{125}I]$IPPI and as expected all AD subjects showed the presence of Tau pathology, whereas all the CN subjects had significantly lower $[^{125}I]$IPPI binding. The AD subjects exhibited more than seven times the amount of binding in the GM compared to CN subjects. There was greater variance in the binding of $[^{125}I]$IPPI in the AD subjects compared to $[^{3}H]$PIB binding. However, all the CN subjects consistently exhibited lower $[^{125}I]$IPPI binding. It should be noted that both $[^{3}H]$PIB incubation and $[^{125}I]$IPPI incubation of the brain slices were done in 10% of alcohol in PBS buffer. Washing of $[^{3}H]$PIB brains were done with 10% of alcohol in PBS buffer, but $[^{125}I]$IPPI brains washing also included 50% of alcohol in PBS buffer. More studies on incubation conditions for $[^{125}I]$IPPI as well as additional subjects may be needed to address the variance in $[^{125}I]$IPPI binding. Additional issues such as potential variance in the binding sites of Tau across subjects will have to be further investigated.

Because of structural features of Tau radioligands with MAO inhibitors, off-target binding of the previously reported radioligands to MAO sites in vivo has caused a concern (Betthauser, 2019). This has resulted in overestimation of Tau. Recent in vitro studies with $[^{18}F]$MK-6240 in AD brain suggests some displacement (up to 20% at high drug concentrations) and may not be a concern for in vivo PET studies (Aguero et al., 2019). Binding of $[^{125}I]$IPPI in brain slices containing AC and CC shown in Figure 8b correlated very well with the presence of Tau, confirmed by anti-Tau Dako A0024 (Figure 8h). Our studies with $[^{125}I]$IPPI showed that at higher concentrations of 10 μM of (R)-deprenyl (for MAO B) and clorgyline (for MAO A), binding was reduced 13% and 20%. At lower concentrations of 1 μM of (R)-deprenyl did not effect $[^{125}I]$ IPPI while 1 μM of clorgyline had a <10% reduction effect on $[^{125}I]$IPPI binding. Thus, small effect of MAO inhibitors on $[^{125}I]$IPPI binding in the AD brain appears to be consistent with the findings of $[^{18}F]$MK-6240 (Aguero et al., 2019). Computational modeling studies of Tau PET radiotracers, including MK-6240 with MAO B suggests potential for some cross-interaction (Murugan et al., 2019).

Since halogens at the six-position of the isoquinoline ring did not have any significant detrimental effect on the binding to Tau, it was expected that BrPPI, the bromine analog of IPPI, would successfully compete with $[^{125}I]$IPPI binding. As seen in Figure 8e, binding of $[^{125}I]$IPPI binding was completely abolished. This suggests that radiobrominated analogs of BrPPI (labeled with ^{75}Br $T_{1/2}$ = 97 min or ^{76}Br $T_{1/2}$ = 16 hr or ^{77}Br $T_{1/2}$ = 3.2 days) may serve as potential PET radiotracers for Tau with longer physical half-life options (DeJesus & Mukherjee, 1988). The extent of displacement of $[^{125}I]$IPPI with unlabeled IPPI and MK-6240 was similarly in excess of 95%. Both PET and SPECT imaging agents of IPPI are possible, provided in vivo stability and kinetics are found appropriate. Iodine-123 IPPI may

serve as a SPECT imaging for Tau, similar to our efforts on imaging nicotinic receptors with iodine-123-labeled niodene (Pandey et al., 2012). For extended PET imaging, iodine-124 IPPI may serve as a PET imaging for Tau (iodine-124 $T_{1/2}$ = 4.2 days) similar to our efforts on extended imaging of dopamine receptors with iodine-124-labeled epidepride (Pandey et al., 2014).

In summary, [^{125}I]IPPI is a stable radioiodinated agent suitable for in vitro studies of Tau. It is a close analog of the currently used PET radiotracer [^{18}F]MK-6240, and is therefore, valuable in carrying out autoradiographic studies in postmortem brain tissues. In vitro binding of [^{125}I] IPPI in transgenic animals of Tauopathy have yet to be conducted. If successful, in vivo PET studies using [^{124}I]IPPI in AD mice models may be considered (Coleman, Liang, Patel, Ali, & Mukherjee, 2017).

ACKNOWLEDGMENTS

Funding information

DATA AVAIL ABILIT Y STATEMENT

The data that support the findings of this study are available from the corresponding author upon reasonable request.

REFERENCES

Aguero C, Dhaynaut M, Normandin MD, Amaral AC, Guehl NJ, Neelamegam R, … Gomez-Isla T (2019). Autoradiography validation of novel Tau PET tracer [F-18]-MK-6240 on human postmortem brain tissue. Acta Neuropathologica Communications, 7(37), 1–15. 10.1186/s40478-019-0686-6 [PubMed: 30606247]

Baranwal A, Patel HH, & Mukherjee J (2014). ^{18}F-Fluorodeoxyglycosylamines: Maillard reaction of ^{18}F-FDG with biological amines. Journal of Labelled Compounds and Radiopharmceuticals, 57(2), 86–91.

Beach TG, Adler CH, Sue LI, Serrano G, Shill HA, Walker DG, … Sabbagh MN (2015). Arizona study of aging and neurodegenerative disorders and brain and body donation program. Neuropathology, 35, 354–389. 10.1111/neup.12189 [PubMed: 25619230]

Betthauser TJ (2019). AD molecular: Imaging Tau aggregates with positron emission tomography. Progress in Molecular Biology and Translational Science, 165, 107–138. [PubMed: 31481160]

Betthauser TJ, Cody KA, Zammit MD, Murali D, Converse AK, Barnhart TE, … Christian BT (2019). In vivo characterization and quantification of neurofibrillary Tau PET radioligand 18F-MK-6240 in humans from Alzheimer disease dementia to young controls. Journal of Nuclear Medicine, 60, 93–99. [PubMed: 29777006]

Braak H, & Braak E (1991). Neuropathological staging of Alzheimer-related changes. Acta Neuropathologica, 82, 239–259. [PubMed: 1759558]

Braak H, Thal DR, Ghebremedhin E, & Tredici KD (2011). Stages of the pathologic process in Alzheimer's disease age categories from 1 to 100 years. Journal of Neuropathology and Experimental Neurology, 70, 960–969. [PubMed: 22002422]

Chen ST, Siddarth P, Merrill DA, Martinez J, Emerson ND, Liu J, … Small GW (2018). FDDNP-PET Tau brain protein binding patterns in military personnel with suspected chronic traumatic encephalopathy. Journal of Alzheimer's Disease, 65, 79–88.

Coleman RA, Liang C, Patel R, Ali S, & Mukherjee J (2017). Brain and brown adipose tissue metabolism in Tg 2576 transgenic mice models of Alzheimer's disease assessed using ^{18}F-FDG PET. Molecular Imaging, 16, 1–9.

Crowther RA (1991). Straight and paired helical filaments in Alzheimer disease have a common structural unit. Proceedings of the National Academy of Sciences, 88(6), 2288–2292. 10.1073/pnas.88.6.2288

DeJesus OT, & Mukherjee J (1988). Radiobrominated m-tyrosine analog as a potential CNS L-Dopa PET tracer. Biochemical and Biophysical Research Communications, 150, 1027–1031. [PubMed: 3257696]

Drake LR, Pham JM, Desmond TJ, Mossine AV, Lee SJ, Kilbourn MR, … Scott PJH (2019). Identification of AV-1451 as a weak, nonselective inhibitor of monoamine oxidase. ACS Chemical Neuroscience, 10, 3839–3846. 10.1021/acschemneuro.9b00326 [PubMed: 31339297]

Fitzpatrick AWP, Falcon B, He S, Murzi AG, Murshudow G, Garringer HI, … Scheres SHW (2017). Cryo-EM structures of Tau filaments from Alzheimer's disease. Nature, 547, 185–190. 10.1038/nature23002 [PubMed: 28678775]

Goedert M, Yamaguchi Y, Mishra SK, Higuchi M, & Sahara N (2018). Tau filaments and the development of positron emission tomography tracers. Front Neurology, 9, 70. 10.3389/fneur.2018.00070

Honer M, Gobbi L, Knust H, Kuwabara H, Muri D, Koemer M, … Borroni E (2018). Preclinical evaluation of 18F-RO6958948, 11C-RO6931643, and 11C-RO6924963 as novel PET radiotracers for imaging Tau aggregates in Alzheimer's disease. Journal of Nuclear Medicine, 59, 675–681. [PubMed: 28970331]

Hostetler ED, Walji AM, Zeng ZP, Miller I, Bennacef C, Salinas B, … Evelhoch JL (2016). Preclinical characterization of 18F-MK-6240, a promising PET tracer for in vivo quantification of human neurofibrillary tangles. Journal of Nuclear Medicine, 57(10), 1599–1606. 10.2967/jnumed.115.171678 [PubMed: 27230925]

Julien C, Marcouiller F, Bretteville A, El Khoury NB, Baillargeon J, Hebert SS, & Planel E (2012). Dimethyl sulfoxide induces both direct and indirect Tau hyperphosphorylation. PLoS One, 7(6), e40020. 10.1371/journal.pone.0040020 [PubMed: 22768202]

Lemoine L, Gillberg P-G, Svedberg M, Stepanov V, Jia Z, Huang J, … Nordberg A (2017). Comparative binding properties of the Tau PET tracers THK5117, THK5351, PBB3, and T807 in postmortem Alzheimer brain. Alzheimer's Research Therapy, 9(96), 1–13.

Leuzy A, Chiotis K, Lemoine L, Gilberg P-G, Almkvist O, Rodriguez-Vieitez E, & Nordberg A (2019). Tau PET imaging in neurodegenerative tauopathies-still a challenge. Molecular Psychiatry, 24, 1112–1134. 10.1038/s41380-018-0342-8 [PubMed: 30635637]

Meng X-Y, Zhang H-X, Mezei M, & Cui M (2011). Molecular docking: A powerful approach for structure-based drug discovery. Current Computer Aided-Drug Design, 7(2), 146–157. [PubMed: 21534921]

Mukherjee J, & Yang ZY (1997). Evaluation of monoamine oxidase B inhibition by fluoxetine (Prozac): An in vitro and in vivo study. European Journal of Pharmacology, 337, 111–114. [PubMed: 9389388]

Mukherjee J, & Yang ZY (1999). Monoamine oxidase A inhibition by fluoxetine: An in vitro and in vivo study. Synapse (New York, N. Y.), 31, 285–289.

Murugan NA, Chiotis K, Rodriguez-Vieitez E, Lemoine L, Agren H, & Nordberg A (2019). Cross-section of Tau PET tracers with monoamine oxidase B: Evidence from in silico modelling and in vivo imaging. European Journal of Nuclear Medicine and Molecular Imaging, 46, 1369–1382. [PubMed: 30919054]

Murugan NA, Nordberg A, & Agren H (2018). Different positron emission tomography Tau tracers bind to multiple binding sites on the Tau fibril: Insight from computational modeling. ACS Chem Neuroscience, 9, 1757–1767.

Ng KP, Pascoal TA, Mathotaarachchi S, Therriault J, Kang MS, Shin M, … Rosa-Neto P (2017). Monoamine oxidase B inhibitor, selegiline, reduces 18-THK5351 uptake in the human brain. Alzheimers Research Therapy, 9(25), 1–9.

Pan ML, Mukherjee MT, Patel HH, Patel B, Constantinescu CC, Mirbolooki MR, … Mukherjee J (2016). Evaluation of [^{11}C]TAZA for amyloid Aβ plaque imaging in postmortem Alzheimer's disease brain region and whole body distribution in rodent PET/CT. Synapse, 70, 163–176. [PubMed: 26806100]

Pandey SK, Pan S, Kant R, Pan ML, Kuruvilla SA, & Mukherjee J (2012). Synthesis and evaluation of ^{123}I-Niodene as potential imaging agent for nicotinic α4β2 receptors. Bioorganic & Medicinal Chemistry Letters, 22, 7610–7614. [PubMed: 23116890]

Pandey SK, Venugopal A, Kant R, Coleman RA, & Mukherjee J (2014). ^{124}I-Epidepride: A high affinity and selective PET radiotracer with potential for extended imaging of dopamine D2/D3 receptors. Nuclear Medicine and Biology, 41(5), 426–431. [PubMed: 24602412]

Villemagne VL, Dore V, Burnham SC, Masters CL, & Rowe C (2018). Imaging Tau and amyloid-b proteinopathies in Alzheimer's disease and other conditions. Nature Reviews, 14, 225–236.

Walji A, Hostetler E, Greshock T, Li J, Moore KP, Bennacef I, … Fu J (2015). WO 2015/188368 A1.

Walji AM, Hostetler ED, Selnick H, Zeng Z, Miller P, Bennacef I, … Coleman PJ (2016). Discovery of 6-(Fluoro-18F)-3-(1H-pyrrolo[2,3-c]pyridine-1-yl)isoquinolin-5-amine ([18F]-MK-6240): A positron emission tomography (PET) imaging agent for quantification of neurofibrillary tangles (NFTs). Journal of Medicinal Chemistry, 59, 4778–4789. [PubMed: 27088900]

Watanabe H, Tatsumi H, Kaide S, Shimizu Y, Iikuni S, & Ono M (2020). Structure-activity relationships of radioiodinated 6,5,6-tricyclic compounds for the development of Tau imaging probes. ACS Medicinal Chemistry Letters, 11, 120–126. [PubMed: 32071677]
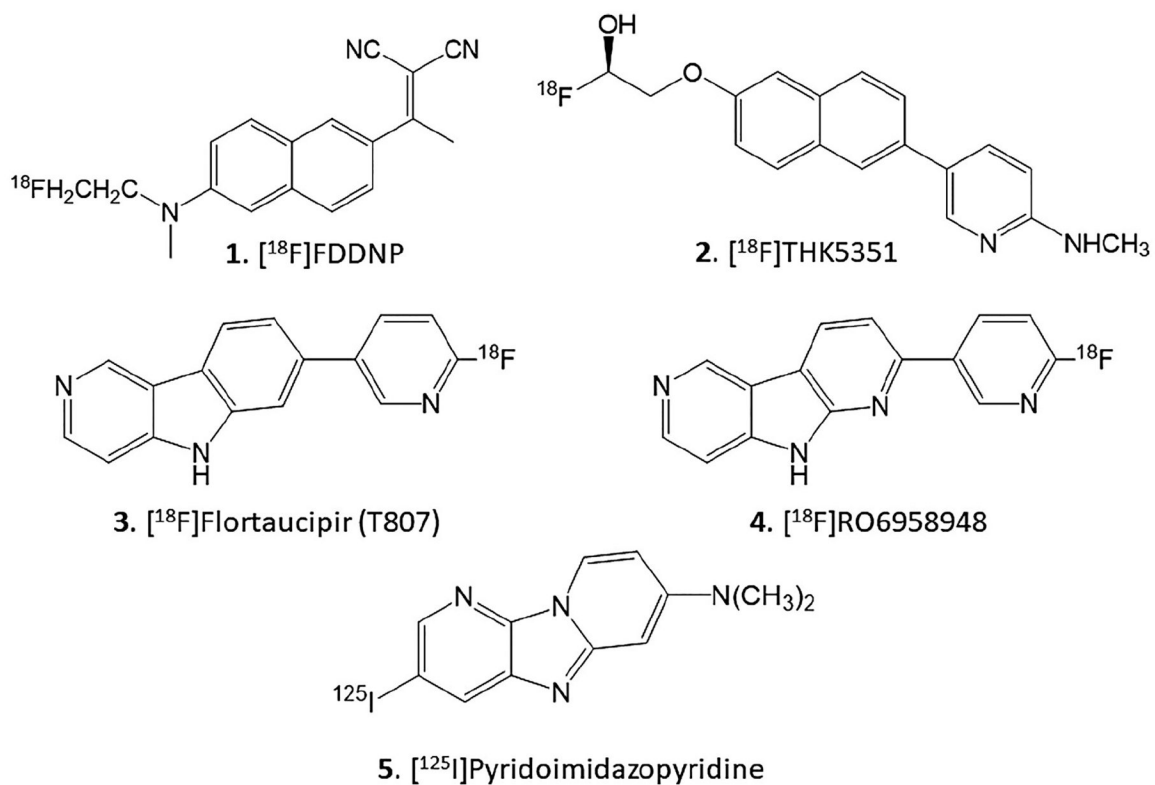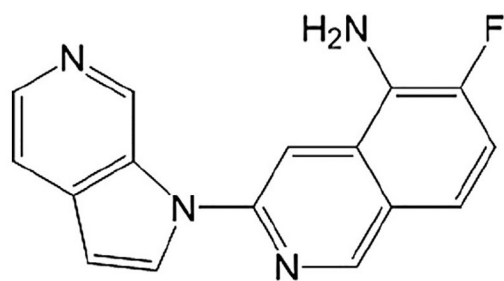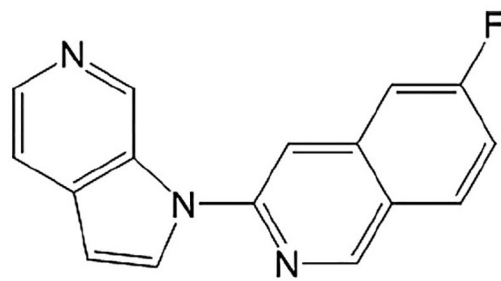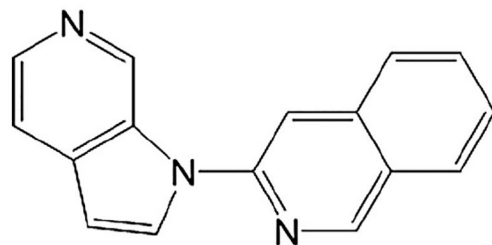
FIGURE 1.
Chemical structures of Tau binding radioligands. **1**. [18F]FDDNP; **2**. [18F]THK5351; **3**. [18F]Flortaucipir (T807); **4**. [18F] RO6958948; **5**. [125I]Pyridoimidazopyridine
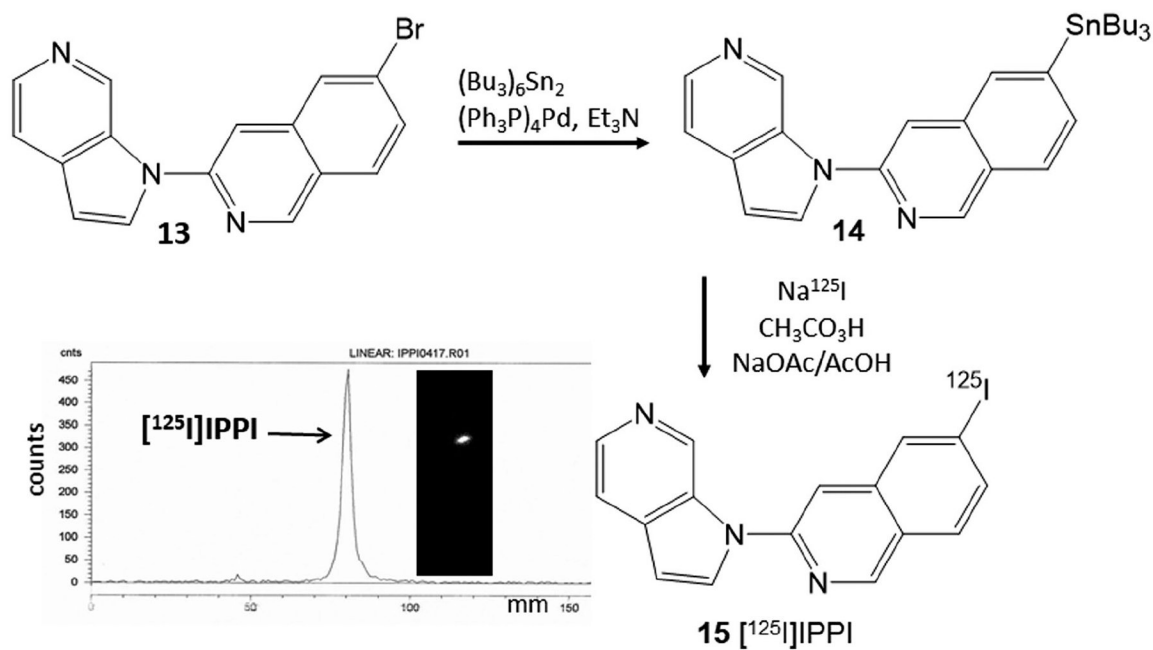
FIGURE 2.
Chemical structures of Tau binding Azaindole derivatives. Substituent effects at the six-position in isoquinoline moiety show small effect on binding affinity. **6.** MK-6240 (Tau Ki = 0.43/0.36 nM); **7.** MK-10 (Tau Ki = 0.22 nM); **8.** MK-H (Tau Ki = 0.54/0.30 nM); **9.** IPPI (Tau Ki = 0.75 nM)
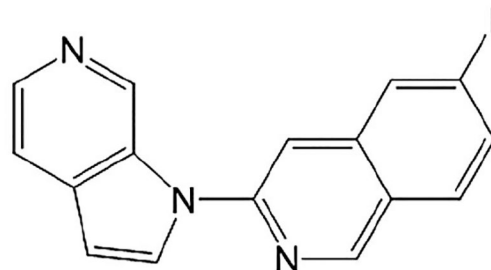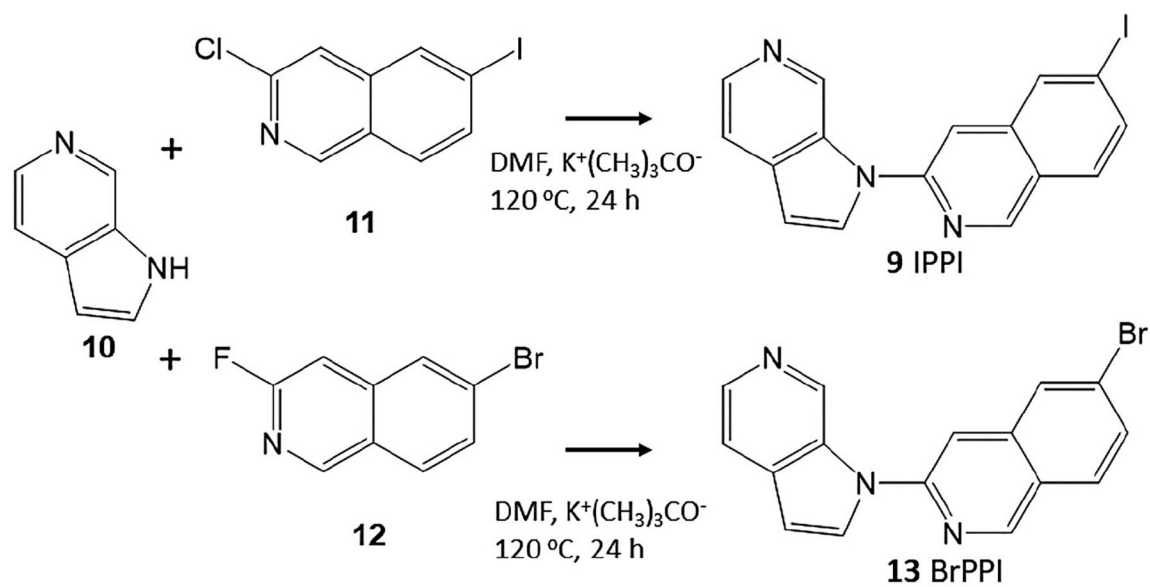
FIGURE 3.
Synthesis of IPPI and BrPPI. Azaindole **10** was reacted with 3-chloro-6-iodoisoquinoline **11** in dimethylformamide (DMF) in the presence of potassium *tert*-butoxide for 24 hr at 120°C to provide IPPI, **9**. Similarly, azaindole **10** was reacted with 3-fluoro-6-bromoisoquinoline **12** in DMF in the presence of potassium *tert*-butoxide for 24 hr at 120°C to provide 6-bromo-3-(1H-pyrrolo[2,3-c] pyridine-1-yl)isoquinoline, BrPPI, **13**

FIGURE 4.

Radiosynthesis of [125I]IPPI. BrPPI, **13** was refluxed with bis(tributyltin) in the presence of tetrakis(triphenylphosphine) palladium(0) for 24 hr to provide 6-tributyltin-3-(1H-pyrrolo[2,3-c]pyridine-1-yl)isoquinoline, **14**. Tin precursor **14** was reacted with sodium [125I]iodide under oxidative conditions using peracetic acid to provide [125I]IPPI, **15**. Thin-layer chromatogram of [125I]IPPI shows purity of >95%
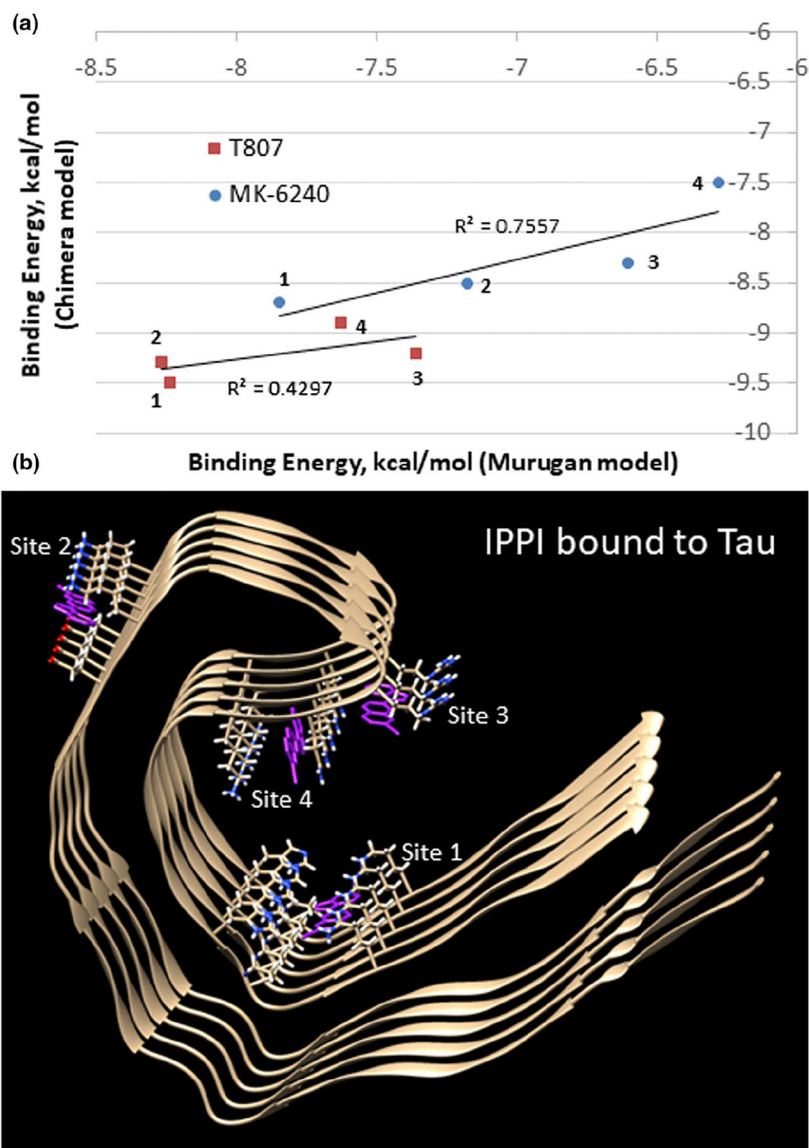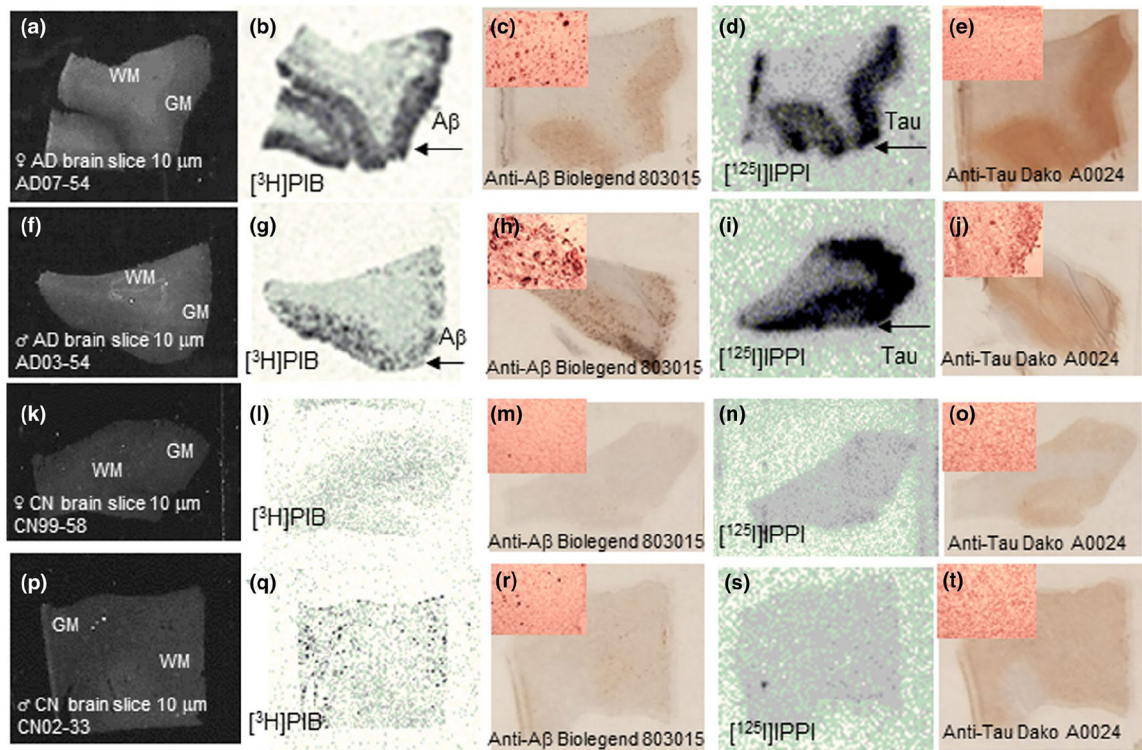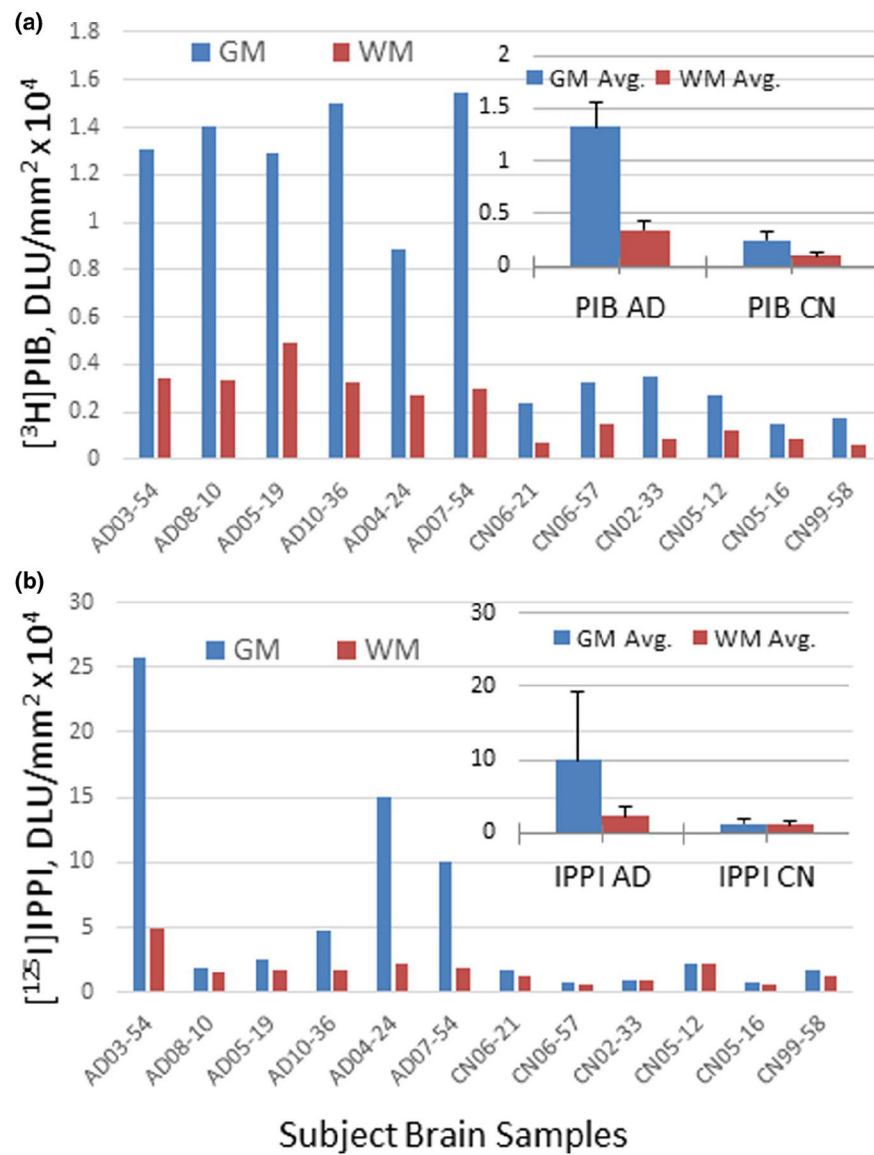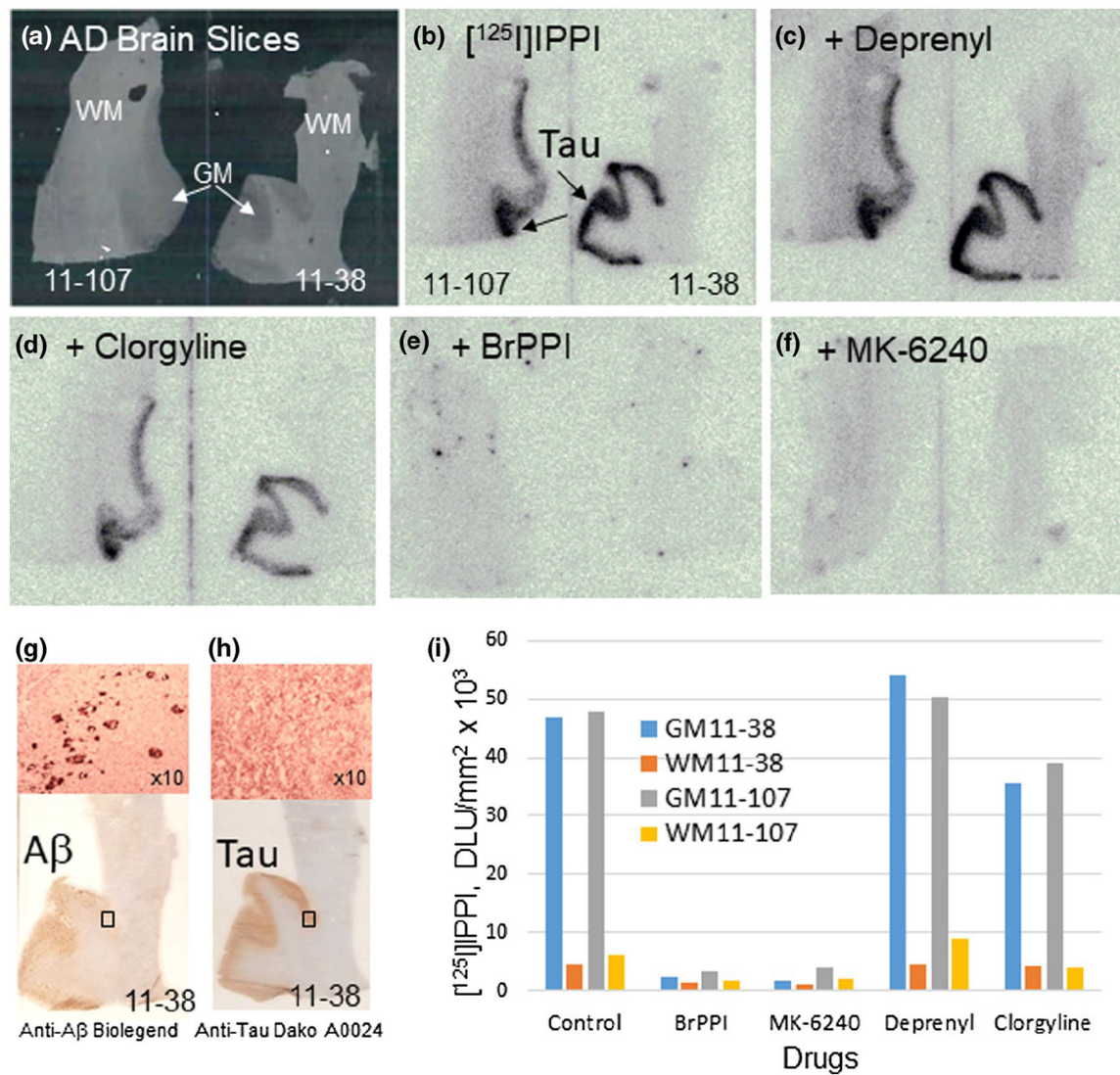
FIGURE 5.
Tau Molecular model. (a) Binding of Tau ligands T-807 and MK-6240 was carried out using a Chimera AD Tau molecular model and efficacy ((kcal/mol) correlated with measures from the reported Murugan model at the four binding sites for each ligand (R^2 = .7989 for MK-6240 and R^2 = .4297 for T807). (b) Chimera AD Tau model showing binding of IPPI (in purple) at the four different binding sites (Site 1, 2, 3, and 4)

FIGURE 6.

Postmortem human brain autoradiography [^{125}I]IPPI. (a,f) Human postmortem AD brain frontal cortex (10 μm thick sections) showing grey matter (GM) and white matter (WM). (b,g) Binding of [^{3}H]PIB to Aβ plaques (shown by arrows) in AD07-54 and AD03-54 frontal cortex sections shown in (a,f). (c,h) Anti-Aβ staining of AD07-54 and AD03-54 showing presence of Aβ plaques. Inset is at ×10 magnification of GM. (d,i) Binding of [^{125}I]IPPI to Tau (shown by arrows) in AD07-54 and AD03-54 frontal cortex sections shown in (a,d). (e,j) Anti-Tau staining of AD07-54 and AD03-54 showing presence of NFT in GM regions. Inset is at ×10 magnification of GM. (k,p) Human postmortem cognitively normal (CN) brain frontal cortex (10 μm thick sections) showing grey matter (GM) and white matter (WM). (l,q) Binding of [^{3}H]PIB to Aβ plaques in CN99-58 and CN02-33 frontal cortex sections shown in (k,P). (M, R) Anti-Aβ staining of CN99-58 and CN02-33 showing absence of Aβ plaques. Inset is at ×10 magnification of GM. (n,s) Binding of [^{125}I]IPPI to Tau in CN1 and CN2 frontal cortex sections shown in (k,p). (o,t) Anti-Tau staining of CN99-58 and CN02-33 showing absence of NFT in GM regions. Inset is at ×10 magnification of GM

FIGURE 7.
Plots showing [^{3}H]PIB and [^{125}I]IPPI in all subjects. (a) Plot shows binding of [^{3}H]PIB to Aβ plaques in GM and WM in 6 AD and 6 CN subjects; Inset shows average of 12 subjects (6 AD and 6 CN) binding of [^{3}H]PIB. (b) Plot shows binding of [^{125}I]IPPI to Tau in GM and WM in 6 AD and 6 CN subjects; Inset shows average of 12 subjects (6 AD and 6 CN) binding of [^{125}I]IPPI

FIGURE 8.

Competition of [125I]IPPI with Drugs. (a) Postmortem human brain 10 μm thick sections (from two AD subjects, 11–107 and 11–38) of anterior cingulate (AC) grey matter (arrows showing GM) and corpus callosum (CC) white matter (WM). (b) [125I]IPPI binding to grey matter, AC with low nonspecific binding in white matter, CC. (c) Deprenyl, 1 μM effect on [125I]IPPI binding. (d) Clorgyline, 10 μM effect on [125I]IPPI binding. (e) BrPPI, 10 μM effect on [125I]IPPI binding. (f) MK-6240, 10 μM effect on [125I]IPPI binding. (g) Immunostaining of 11–38 with anti-Aβ Biolegend 803,015 for Aβ plaques of entire slice and magnification of box (×10 inset). (h) Immunostaining of 11–38 with anti-Tau Dako A0024 for total Tau of entire slice and magnification of box (×10 inset). (i) Plot comparing GM and WM in the two AD subjects with different drugs
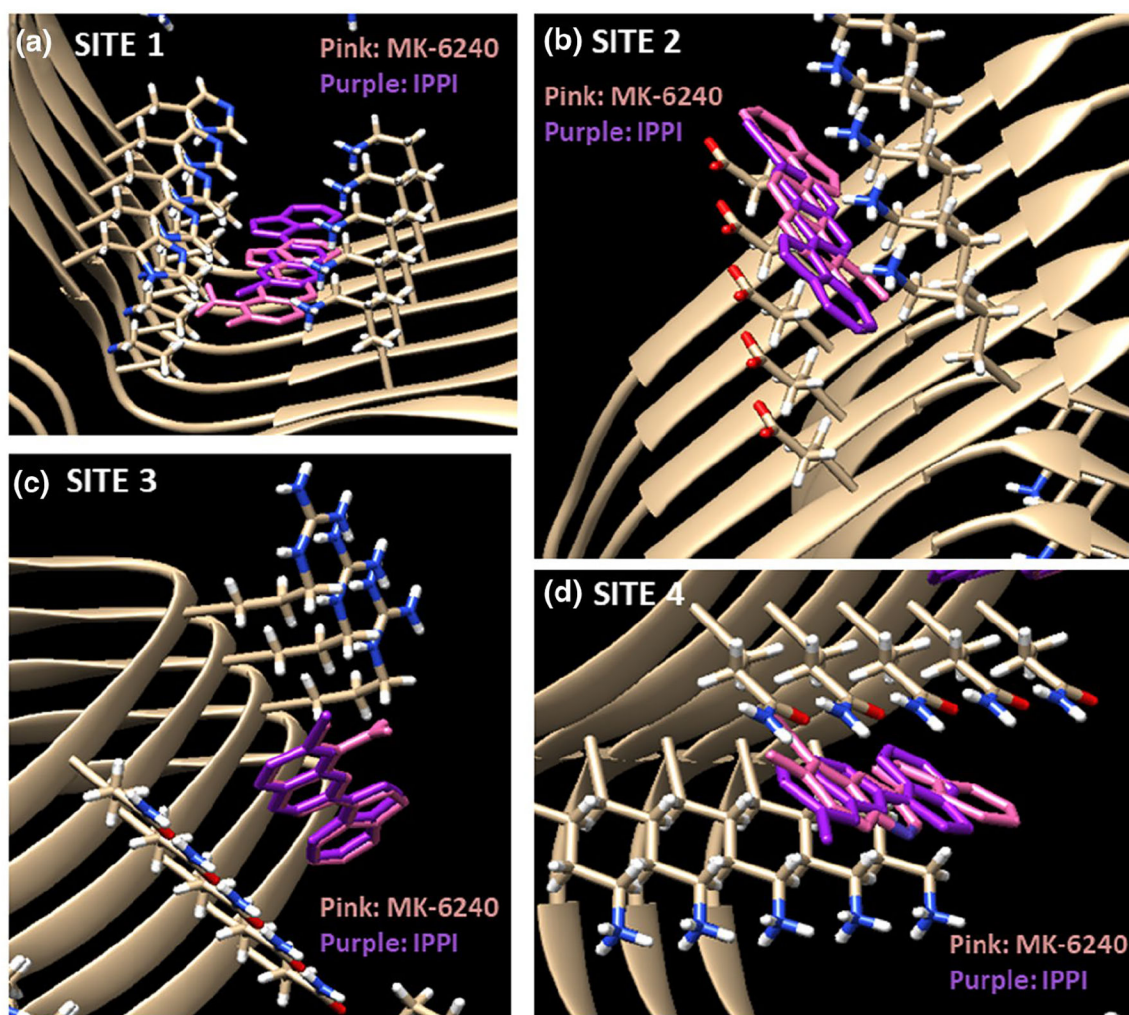
FIGURE 9.
Comparison of MK-6240 and IPPI at Tau Binding Sites using Chimera model. (a) Binding of MK-6240 (pink, −8.7 kcal/mol) and IPPI (purple, −7.8 kcl/mol) at Site 1. (b) Binding of MK-6240 (pink, −8.5 kcal/mol) and IPPI (purple, −8.1 kcal/mol) at Site 2. (c) Binding of MK-6240 (pink, −8.3 kcal/mol) and IPPI (purple, −8.2 kcal/mol) at Site 3. (d) Binding of MK-6240 (pink, −7.5 kcal/mol) and IPPI (purple, −7.5 kcal/ mol) at Site 4

TABLE 1

Patient samples and data[a]

ID	Pathology	Gender	Age expired	Brain region	Plaque total	Tangle total	Braak score
06–21	CN	Male	73	Frontal Cortex	5.5	4.5	II
05–16	CN	Male	82	Frontal Cortex	4	3	III
02–33	CN	Male	85	Frontal Cortex	8.25	5	III
06–57	CN	Male	92	Frontal Cortex	8	4.5	III
05–12	CN	Female	88	Frontal Cortex	6.25	2.5	III
99–58	CN	Female	91	Frontal Cortex	1	4	III
03–54	AD	Male	76	Frontal Cortex	11.75	15	V
04–24	AD	Male	78	Frontal Cortex	13.25	15	VI
10–36	AD	Male	90	Frontal Cortex	15	15	V
05–19	AD	Female	75	Frontal Cortex	15	13.5	V
07–54	AD	Female	82	Frontal Cortex	15	15	VI
08–10	AD	Female	87	Frontal Cortex	13	14	V
11–107	AD	Male	71	Anterior Cingulate	14	15	VI
11–38	AD	Male	64	Anterior Cingulate	14.5	15	VI

[a]Frozen brain samples were obtained from Banner Sun Health Institute, Sun City Arizona (Beach et al., 2015); AD, Alzheimer's disease; CN, cognitively normal and may include mild cognitive impairment (MCI) subjects; Plaque total, Includes neuritic, cored, and diffuse, in frontal, temporal, parietal, hippocampal, and entorhinal cortex. Semiquantitative scores of none, sparse, moderate, and frequent were converted to numerical values 0–3 for each region and summed to provide Plaque total; Tangle total: neurofibrillary tangle density in frontal, temporal, and parietal lobes, hippocampal CA1 region and entorhinal cortical regions. Numerical values 0–3 for each region were summed to provide Tangle total; Braak score, Braak neurofibrillary stage (0–VI) defined in Braak and Braak (1991).

TABLE 2

Molecular modeling measures

Tau ligand	Site 1 Kcal/mol	Site 2 Kcal/mol	Site 3 Kcal/mol	Site 4 Kcal/mol	Binding affinity, Ki nM
MK-6240[a]	−8.7	−8.5	−8.3	−7.5	0.43/0.36[d]
	−7.85[b]	−7.18[b]	−6.60[b]	−6.28[b]	
T-807[a]	−9.5	−9.3	−9.2	−8.9	0.30[e]
	−8.24[b]	−8.27[b]	−7.36[b]	−7.63[b]	
IPPI[a]	−7.8	−8.1	−8.2	−7.5	0.75[c]

[a]Chimera molecular models of Tau and AutoDock used to measure binding of the Tau ligands.

[b]Reported binding parameters of the Tau ligands (Murugan et al., 2018).

[c]Affinity of MK-6240 (Walji et al., 2015, 2016).

[d]Affinity of T807 (Nordberg et al., 2019).

[e]Affinity of IPPI (Walji et al., 2015).